Electrochimica Acta 349 (2020) 136356

Contents lists available at ScienceDirect

Electrochimica Acta

journal homepage: www.elsevier.com/locate/electacta

An effective electrolyte design to improve the high-voltage performance of high-capacity NCM811 / SiO_x-Gr batteries

Xiangbang Kong , Junjie Liu , Yige Zhang , Jing Zeng , Jinbao Zhao *

State Key Laboratory of Physical Chemistry of Solid Surfaces, Collaborative Innovation Centre of Chemistry for Energy Materials, State-Province Joint Engineering Laboratory of Power Source Technology for New Energy Vehicle, Engineering Research Center of Electrochemical Technology, Ministry of Education, College of Chemistry and Chemical Engineering, Xiamen University, Xiamen, 361005, PR China

A R T I C L E I N F O

Article history:
Received 7 March 2020
Received in revised form
28 April 2020
Accepted 28 April 2020
Available online 29 April 2020

Keywords:
$LiNi_{0.8}Co_{0.1}Mn_{0.1}O_2$
Silicon oxide-graphite
High-voltage performance
Electrolyte
Lithium-ion batteries

A B S T R A C T

Increasing the charge voltage of a battery can greatly augment its specific capacity, but the increase of the voltage often brings some negative effects. Among them, the decomposition of the electrolyte at high voltage is a very serious problem. In this work, theoretical calculations are used to combine the advantages of each solvent, so that the designed electrolyte can effectively strengthen the high-voltage property of high-capacity NCM811/SiO_x-Gr system batteries. The additive sulfolane is adopted to be oxidized in advance and build a protective film around the $LiNi_{0.8}Co_{0.1}Mn_{0.1}O_2$ positive electrode, and fluoroethylene carbonate is employed to be priorly reduced and form a film on the face of silicon oxide-graphite negative electrode. Compared with the traditional electrolyte, the cycling retention rate of the full battery is increased from 58.44% to 77.51% after cycling for 200 times under the voltage of 4.5 V with the high-performance electrolyte. From the results of a series of tests, it can be found that the high-voltage electrolyte can effectually maintain the structural of the cathode and anode materials at high voltages and improve the electrochemical performance. In addition, the electrolyte also has high conductivity and wettability with separator, which brings it a good application prospect.

1. Introduction

In recent years, as the energy crisis and environmental problems continue to intensify, clean energy and energy storage equipment are receiving more and more attention [1,2]. Among them, lithium-ion batteries have become the first choice for portable electronic equipment and environmentally-friendly hybrid vehicles because of their high energy density and long cycle life [3–5]. With the development of science and technology, people's requirements for the battery (especially power batteries) endurance are increasing [6,7], which requires cathode and anode materials with higher energy density. For positive electrode materials, layered $LiNi_xCo_yMn_{1-x-y}O_2$ (NCM) materials with high nickel content are sought after for their advantages such as high specific capacity and high power density [8,9]. For negative electrode materials, silicon-based materials can provide significantly higher capacity than traditional graphite negative electrode materials [10–13]. So combining high nickel $LiNi_{0.8}Co_{0.1}Mn_{0.1}O_2$ (NCM811) cathode materials with silicon oxide-graphite (SiO_x-Gr) anode materials will bring a battery system with higher capacity [14,15]. Despite this, people are still not satisfied with the current battery capacity, hoping to increase the actual battery capacity by increasing the charge voltage [16]. However, after increasing the charge voltage of the battery, many practical problems will be encountered. For example, it is difficult for the normal electrolyte to work under high voltage. When the battery's charge voltage is high, the electrolyte often suffers from severe oxidation. And some side products during the cycling will form on the surface of the electrode material, resulting in a significant decrease in battery cycle performance [17]. When the charge voltage of the battery is too high, the degree of delithiation of the layered positive electrode material continues to deepen. As primary particles go through larger volume changes during intercalation and deintercalation of lithium ion, secondary particles usually produce more pronounced cracks during charge and discharge cycles, leading to significant structural damage. At the same time, excessive deintercalation of lithium ion will bring serious phase changes, which can cause the transition metal ions to dissolve and desorb from the layered structure, which will critically affect battery performance [18]. For silicon-based anode materials,

* Corresponding author.
E-mail address: jbzhao@xmu.edu.cn (J. Zhao).

https://doi.org/10.1016/j.electacta.2020.136356
0013-4686/

the volume effect is more obvious in the case of deep lithium ion insertion. The internal stress caused by volume expansion and contraction will lead to structural damage to the anode materials and capacity decay [19–21]. In order to cope with this problem, people often use high-voltage-resistant electrolytes. On one hand, the decomposition of the electrolyte under high voltage is solved. On the other hand, the electrolyte is used to protect the positive and negative materials, mitigating damage of the positive and negative materials under high voltage [22–24]. However, the research of high-voltage electrolytes often tends to focus on the performance of half-cells. As a result, many high-voltage electrolytes only improve the high-voltage performance of one electrode but have poor compatibility with another electrode, which greatly affects the practical application of the electrolytes. Therefore, it is necessary to develop an electrolyte that can effectively protect the positive and negative electrodes materials at the same time under high voltage.

In this work, theoretical calculations were used to screen out suitable solvent components. HFE (fluoroethylene propylene ether) and FEC (fluoroethylene carbonate) were selected to increase the oxidation resistance of the electrolyte. Good film-forming performance of FEC can improve the compatibility of electrolyte with silicon-based anodes, it can stabilize silicon-based anode by depositing an irreversible polymer layer [25]. In addition, SL (sulfolane) was adopted as the cathodes film forming additive to form a steady protective layer on the surface of the positive electrodes, and DMC (dimethyl carbonate) was employed to lower the viscosity of the electrolyte. On this basis, a high voltage electrolyte was prepared. Through experimental tests, the designed electrolyte can effectively protect the anode and cathode materials to increase battery capacity retention of the NCM811/SiO_x-Gr full batteries, showing a much improved high voltage electrochemical performance compared to traditional electrolyte.

2. Experiment section

2.1. Density functional theory calculation

The calculation part of this work was run on the Gaussian09 software package. Based on this, all structures (including the steady state and transition state) were analyzed and optimized, and NBO (natural bond orbital) charge distribution analysis was also taken into account. At the same time, in order to study the influence of solvents in the entire system, we use a continuous-mode polarization model CPCM (conductor-variant polarized continuum model) to optimize the structure of the equilibrium state.

2.2. Preparation of electrolyte

In this work, two different electrolytes were prepared. One is a commonly used conventional electrolyte, and the other is the designed high voltage electrolyte. In the preparation of traditional electrolytes, ethylene carbonate (EC) was mixed with DMC according to the mass ratio of 1: 1. After that, 1 M $LiPF_6$ was added to the prepared solution. For the convenience of expression, this electrolyte is hereinafter referred to as LB-301 electrolyte. When preparing high-voltage electrolyte, DMC, SL, FEC and HFE were mixed according to the mass ratio of 30: 30: 20: 20, and after being stirred to form a uniform solution, 1 M $LiPF_6$ was also added thereto. After standing for 12 h, the designed high voltage electrolyte is obtained, which is referred to as SL electrolyte hereinafter.

2.3. Battery assembly and electrochemical testing

The positive and negative electrodes used in this experiment were provided by Tianjin JEVE Power Co., Ltd. The composition of the positive electrodes is 97.75 wt% NCM811, 0.75 wt% CNTs, 0.5 wt % SuperP, and 1 wt% PVDF. The composition of the negative electrodes is 84.92 wt% graphite, 10.5 wt% silicon oxide, 0.2 wt% CNTs, 0.8 wt% SuperP, 1.08 wt% CMC, and 2.5 wt% SBR. The loading density of the cathode materials is about 22 $mg \cdot cm^{-2}$, the areal capacities of cathode and anode are 4.84 $mAh \cdot cm^{-2}$ and 5.27 $mAh \cdot cm^{-2}$ respectively, and the N/P ratio is about 1.09. In the process of battery assembly, the above mentioned positive and negative electrodes, Asahi Kasei polyethylene separator were used. The prepared LB-301 and SL electrolyte were added to the battery separately, and assembled into a CR-2032 coin cells in a glove box under Ar gas atmosphere.

The charge and discharge device used was a Neware test system. In the charge and discharge test, batteries assembled using two kinds of electrolytes were charged and discharged in the voltage range of 2.75–4.4 V and 2.75–4.5 V, respectively. In order to verify the oxidation and reduction properties of LB-301 and SL electrolytes, the LSV (Linear sweep voltammetry) test were carried out from the open circuit potential to 6.0 V and 0 V respectively on each of the two electrolytes. The test was performed with an electrochemical workstation and a three-electrode system at the scanning speed of 0.1 $mV \cdot s^{-2}$. The working electrode was a Pt electrode, lithium metal was used as the counter electrode and the reference electrode.

2.4. Battery and material characteristics analysis

Solartron was used to test the AC impedance properties of the batteries. SEM (Scanning electron microscope) was applied to display the changes in the morphology of the electrode materials before and after cycling. XRD (X-ray diffraction) was adopted to show the structural change of the electrode materials. TEM (Transmission Electron Microscope) was carried out to study the morphology and structure, and Raman spectra test was used to characterize changes in the cycled cathode materials.

3. Result and discussion

3.1. Theoretical calculation of electrolyte and LSV test

The molecular formula of the solvent used in this experiment is shown in Fig.S1. The HOMO and LUMO energy levels of a solvent are closely related to the solvent's redox property. The higher the HOMO energy level often means stronger oxidation ability, and the lower the LUMO energy level represents stronger reduction ability. The Gaussian09 software package was employed to compute the HOMO and LUMO energy levels of the substances. The results are displayed in Fig.S2 and Tab.S1. The calculation results suggest that the SL has the highest HOMO energy level, so it is the easiest to be oxidized and construct a protective layer around the cathode materials during the charge and discharge process and make a protecting layer. The LUMO energy level of FEC is the lowest, so it is the easiest to be reduced and build a film on the face of the anode materials, which brings a better protection for the negative electrode materials. The working schematic diagram of the prepared electrolyte is shown in Fig. 1. The corresponding components in the electrolyte are expected to protect the cathode and anode materials respectively, which can greatly improve the cycling stability of the NCM811/SiO_x-Gr system battery under high voltage.

At the same time, Fig. 2 shows the LSV test results performed on the two electrolytes. Fig. 2b and c are positive scan results. The LSV test result clearly shows that compared with the traditional LB-301 electrolyte, the designed SL high voltage electrolyte is indeed more easily oxidized with the increase of the scanning potential. From Fig. 2c, the SL electrolyte is truly more easily reduced with the

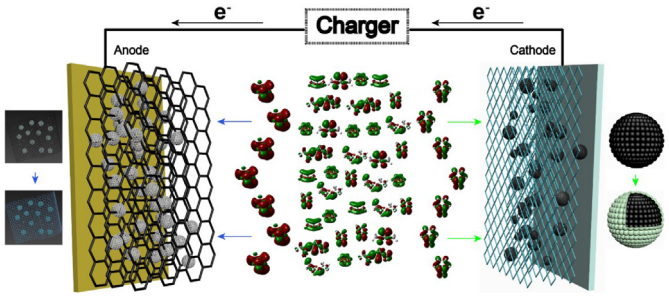

Fig. 1. Schematic diagram of the working principle of SL high voltage electrolyte.

decrease of the scanning potential. This is also in keeping with our previous design outlook, indicating that the SL electrolyte can be preferentially decomposed under cycling conditions to protect the electrode materials.

In actual production, the conductivity of the electrolyte and the wettability of the electrolyte and the separator have a great impact on its battery performance and practicality. The conductivity of the SL electrolyte is around 11.5 mS cm^{-1} at room temperature, similar to that of the LB-301 electrolyte. The contact angle tests were performed on LB-301 and SL electrolytes with the Asahi Kasei separator (Fig.S3). It turned out that the contact angle between the SL electrolyte and the separator was smaller, which indicates that its wettability with the separator is better than that of the LB-301 electrolyte.

3.2. Electrochemical performance

The full batteries using two electrolytes were firstly cycled at a high voltage range of 2.75–4.4 V at a rate of 0.5C, and the electrochemical test results are shown in Fig.S4. It shows that when using the LB-301 electrolyte, the cycling performance of the NCM811/SiO_x-Gr battery decays very quickly, while the cycling performance of the battery using the SL electrolyte is significantly improved. After 200 cycles, the discharge capacity of the full battery was significantly maintained (the cycle retention rate of batteries using different electrolytes is shown in Tab.S2), which indicates the SL electrolyte can protect the electrode materials under high voltage better as expected, thereby efficaciously enhancing the cycling performance of the battery. Based on the above results, the electrochemical cycling of batteries with different electrolyte systems were performed at a higher voltage scope of 2.75–4.5 V. Then AC impedance test (Fig. 3) was conducted on the batteries after cycling to verify the resistance change of the batteries with two electrolytes.

Fig. 3 confirms that when cycling at a voltage of 2.75–4.5 V, batteries using SL electrolyte have higher capacity retention and coulombic efficiency. From Tab.S2, when cycling at a higher voltage of 4.5 V, the cycling retention rate of the battery using the LB-301 after cycling 200 times is only 58.44%, while the battery using SL electrolyte reaches 77.51%, which has significantly improved. At the same time, by analyzing the charge and discharge curves at different cycles, it is found that when using the LB-301 electrolyte, the initial discharge voltage is continuously decreasing as the cycle progresses, which means that as the cycle continues, impurity components are formed on the electrode material surface due to the decomposition behavior of the electrolyte, and ionic/electronic conductivity of these components is low, so that the impedance of the battery will increase, resulting in a decrease in battery capacity and initial discharge voltage [26,27]. In order to verify the results of this experiment, AC impedance tests of two types of discharged batteries after 200 cycles were performed. The frequency range in the impedance test was 0.01–10^5Hz. The fitting results are shown in Tab.S3. The test results exhibit that after 200 cycles, the impedance of the battery with the LB-301 electrolyte is remarkably larger. In the Nyquist diagram, two obvious semicircles appear in the impedance test results. According to previous research, the semicircle in the high frequency region corresponds to the impedance of lithium ions passing through the SEI (solid electrolyte interface) (R_{sei}), the semicircle in the lower frequency region corresponds to the battery's charge transfer impedance (R_{ct}) [28–31]. By fitting the measured impedance results, it is obvious that when using SL electrolyte, both the R_{sei} and R_{ct} values in the impedance results were significantly lower. This means that when the SL electrolyte is used, the content of impurities generated by the disintegration of the electrolyte is lower at the interface of the active material, so lithium ions can easily pass through the solid electrolyte interface, resulting in a smaller value of R_{sei}. Meanwhile, the structure of the electrode material can be better protected, so lithium ions can transfer more easliy in the electrode materials, so the value of R_{ct} is smaller. Therefore, through the EIS test, the SL electrolyte is confirmed to be able to inhibit the continuous disintegration of the electrolyte under high working voltage during cycling, and protect the electrode material well effectively to improve the NCM811/SiO_x-Gr battery cycle performance at high voltage.

3.3. Mechanism analysis

In order to further understand the changes in the cycled electrodes with two electrolytes, the cycled batteries were disassembled and performed with various physical property analysis tests. Firstly, in order to observe the changes in the electrode material morphology before and after cycling in different electrolytes, SEM tests were performed before and after cycling. For seeing the microscopic characteristics more clearly, the cycled electrodes were washed with DMC solvent. The SEM images of the positive

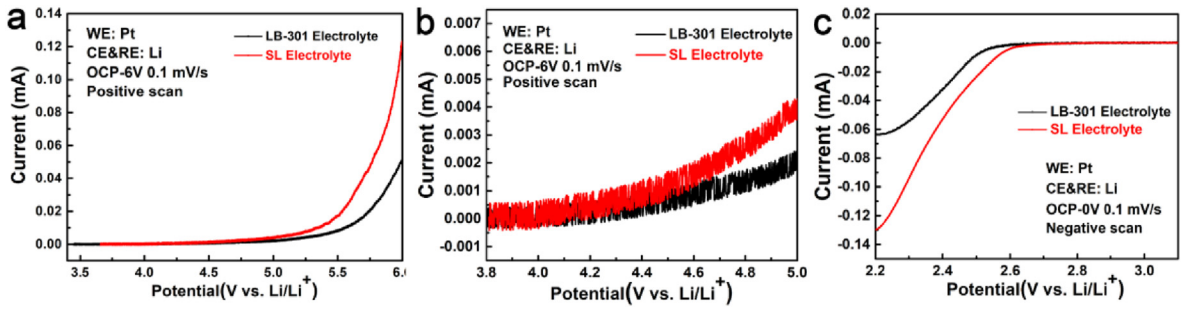

Fig. 2. (a) The positive scan LSV test results of two electrolytes, (b) the partially enlarged plot of positive scan LSV test, (c) The negative scan LSV test results of two electrolytes.

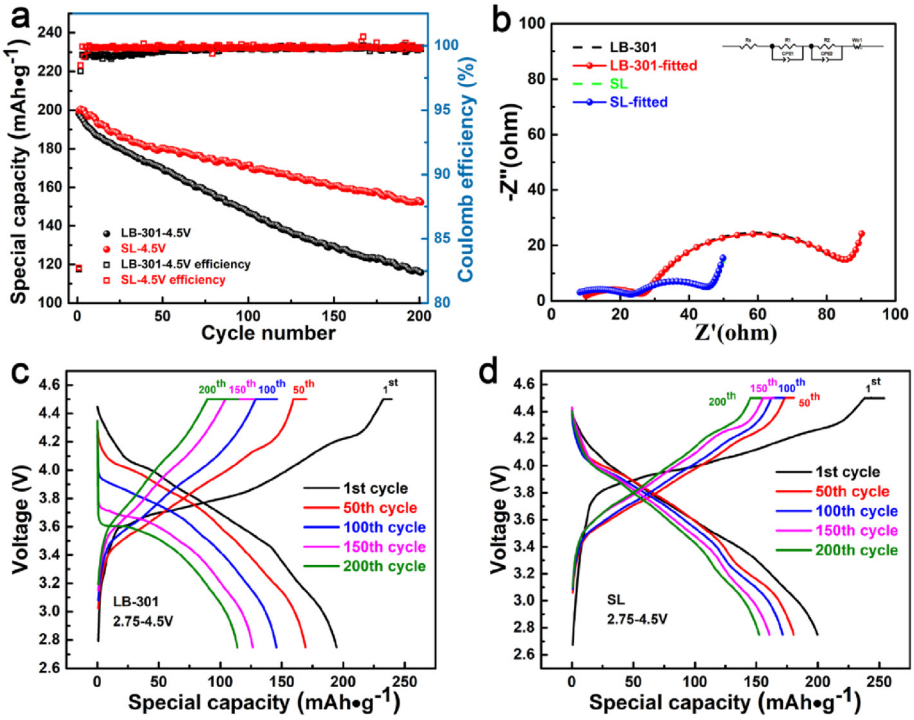

Fig. 3. Cycling performance at a voltage of 2.75–4.5 V (a), impedance test results after 200 cycles (b) and different cycle charge-discharge curves (c, d) of batteries with two electrolytes.

electrode NCM811 materials after cycling under the voltage of 2.75–4.4 V are shown in Fig.S5. From Fig.S5a, the original uncycled NCM811 material is microspheres with regular shapes. After 200 cycles with the LB-301 electrolyte (Fig.S5b), some particles of the original intact microsphere materials were broken. The positive electrode material was broken from the previous densely packed secondary particle spheres into a clearly visible primary particle. This indicates that the positive electrode materials underwent severe volume change in the case of long-term deep deintercalation of lithium ion, which caused the materials to crack and the battery performance to degrade. While using the SL electrolyte (Fig.S5c), it is found that only a few positive electrode particles were broken, and most of the positive material particles maintained a complete spherical shape. When the cycling upper-cutting voltage of the battery was further increased to 4.5 V, this phenomenon is even more obvious, the test results of which are displayed in Fig. 4. After cycled with the LB-301 electrolyte at a cut-off voltage of 4.5 V, according to the SEM images (Fig. 4b), most of the positive electrode materials were severely broken and cracked from the original secondary particles to single primary particles. This situation is very detrimental to the NCM811 materials, because the exposed fresh primary particles may continue to react with the electrolyte, thereby consuming more electrolyte and generating more side reaction impurities, further affecting battery performance [32–34]. In contrast, with the SL high-voltage electrolyte, only a small part of the NCM811 materials were broken (Fig. 4c). It should be that the sulfolane decomposed under high voltage to produce a regular and continuous protective film, which effectively suppressed the collapse of the NCM811 materials and further decomposition of the electrolyte [35]. The comparision of SEM tests suggests that the SL electrolyte can protect the positive electrode materials effectively under high voltage.

In addition, SEM tests were also performed on SiO_x-Gr anode materials before and after cycling. The electrodes cycled under 2.75–4.4 V are shown in Fig.S6. The electrodes cycled under 2.75–4.5 V are compared in Fig. 5. From the SEM results, whether at the cut-off voltage of 4.4 V (Fig.S6b) or 4.5 V (Fig. 5b), The SiO_x-Gr negative electrodes with LB-301 electrolyte showed obvious cracks after cycling for 200 times, and it was accompanied by the crushing of the electrode material, which means that after a deep deintercalation of lithium ion, the SiO_x-Gr anode underwent a serious volume change and cracked. This phenomenon often occurs in the cycle of SiO_x-Gr anodes [10,11,21,36]. In contrast, the SiO_x-Gr negative electrodes after cycling with SL electrolyte under the voltage of 2.75–4.4 V (Fig.S6c), the overall morphology and structure of the electrode material was well maintained, and almost no visible cracks were found. After cycling at 2.75–4.5 V (Fig. 5c), some micro-cracks also appeared on the surface of the negative electrodes, but compared with the negative electrodes with LB-301 under the same conditions, the degree of cracking was significantly lower, indicating that with SL electrolyte, the SiO_x-Gr anodes were well protected during high voltage cycling.

In order to further study the surface interface of the materials before and after cycling, TEM tests were performed on the cathode and anode materials after 4.5 V cycling. The TEM images of NCM811 materials after cycling with LB-301 and SL electrolytes are exhibited in Fig. 6. Fig. 6a–c are the NCM811 after circulating in the LB-301 electrolyte, and Fig. 6d–f are the NCM811 after cycling in the SL electrolyte. For $LiNi_xCo_yMn_{1-x-y}O_2$ ternary cathode materials, it has a good layered structure [37,38]. From Fig. 4b, the NCM811 materials were severely broken after a long cycle in the LB-301 electrolyte, so only small broken particles can be easily found in the TEM test. By observing Fig. 6a–c, the outer surface of the NCM811 material was formed with uneven-thickness impurity components due to the decomposition of the electrolyte, the thickness of the impurity layer ranged from 10 nm to 50 nm. And Fourier transform analysis was made on the near surface area of the cathode material. From Region2 in Fig. 6b and c, for the NCM811

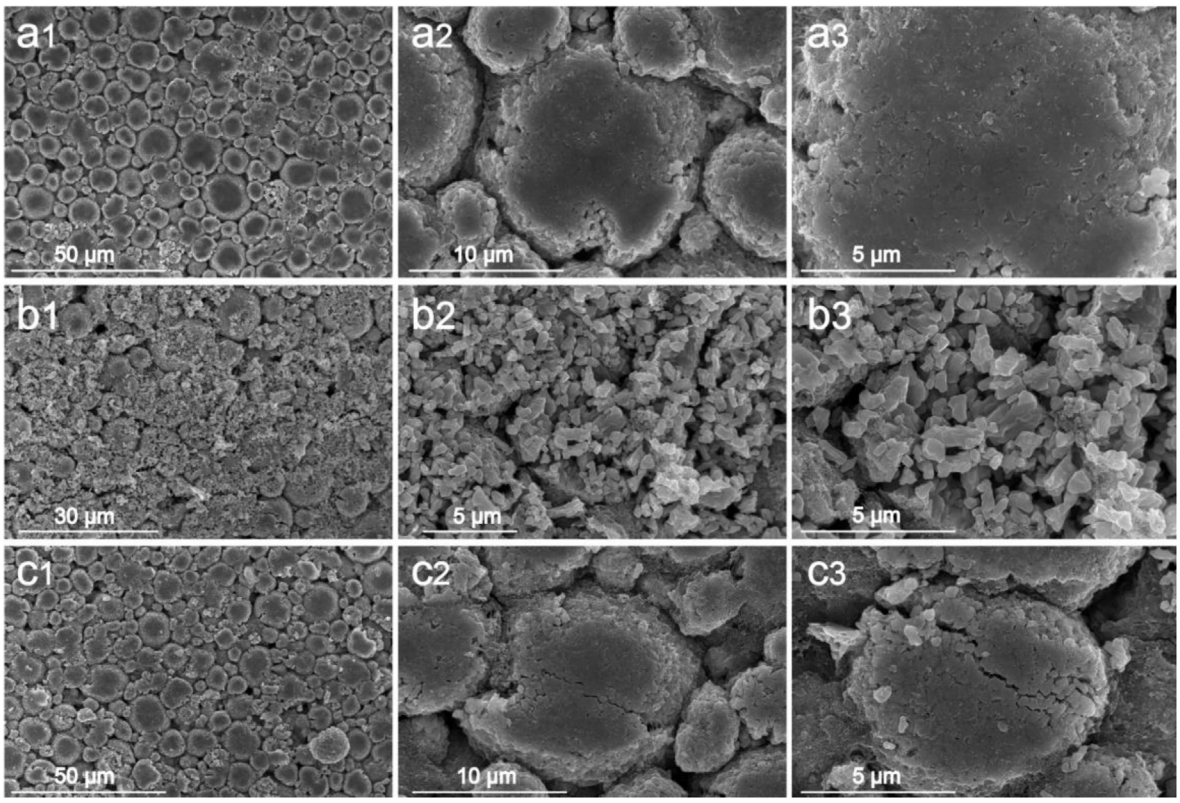

Fig. 4. The pristine NCM811 electrode(a), and the electrode cycled after 200 times from 2.75 to 4.5 V with LB-301 (b) and SL electrolyte (c), respectively.

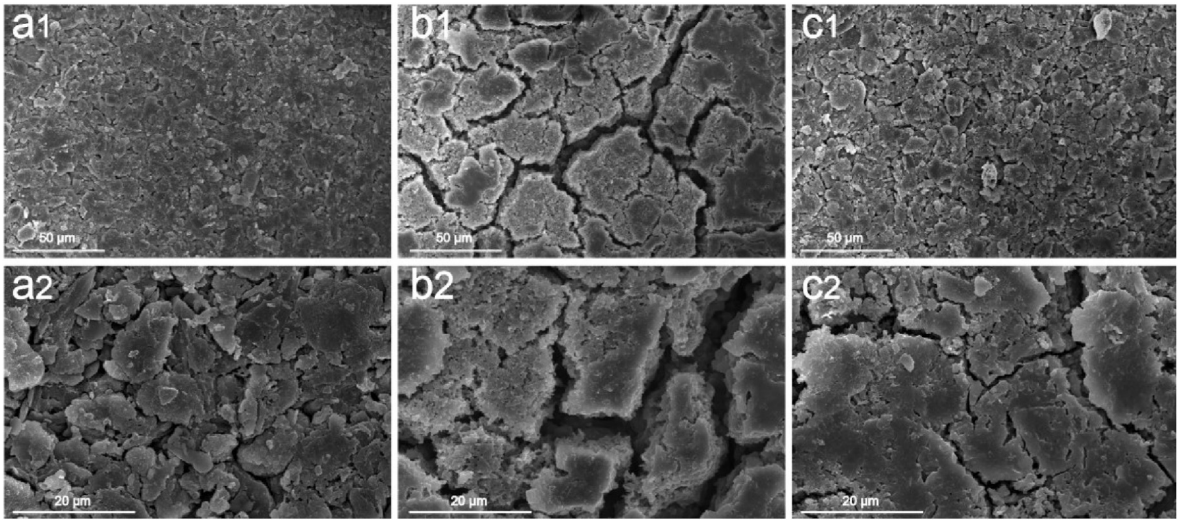

Fig. 5. The pristine SiO_x-Gr electrode(a), and the SiO_x-Gr electrode cycled after 200 times under the voltage of 2.75–4.5 V with the LB-301 (b) and SL electrolyte (c), respectively.

material subjected to high voltage circulating in LB-301 electrolyte, the material structure changed from the original layered to rock salt. And in Region1 of Fig. 6b, the area closer to the interior of the material, there was a mixed structure of layered and rock salt [39–41]. After further studying Region1 in Fig. 6c, it is found that there were corrosion holes in the near surface area, which may be due to the release of oxygen from the NCM811 material at high voltage and the dissolution of transition metals due to electrolyte erosion [42–44]. Furthermore, from Fig. 6d–f, it is apparent that when the SL electrolyte was used, after 200 cycles under high voltage, the NCM811 material still maintained a relatively good spherical topography. In addition, a neat and uniform protective film was formed and the NCM811 particle maintained a good layered structure in the near surface area of the material. Therefore, from the TEM test results, it is proved that the SL electrolyte can protect the structure of the NCM811 materials under high voltage conditions.

The TEM test results of the fresh SiO_x-Gr anode materials and the SiO_x-Gr anodes after circulating in LB-301 and SL electrolytes are shown in Fig. 7. From Fig. 7a, it can be clearly seen that the

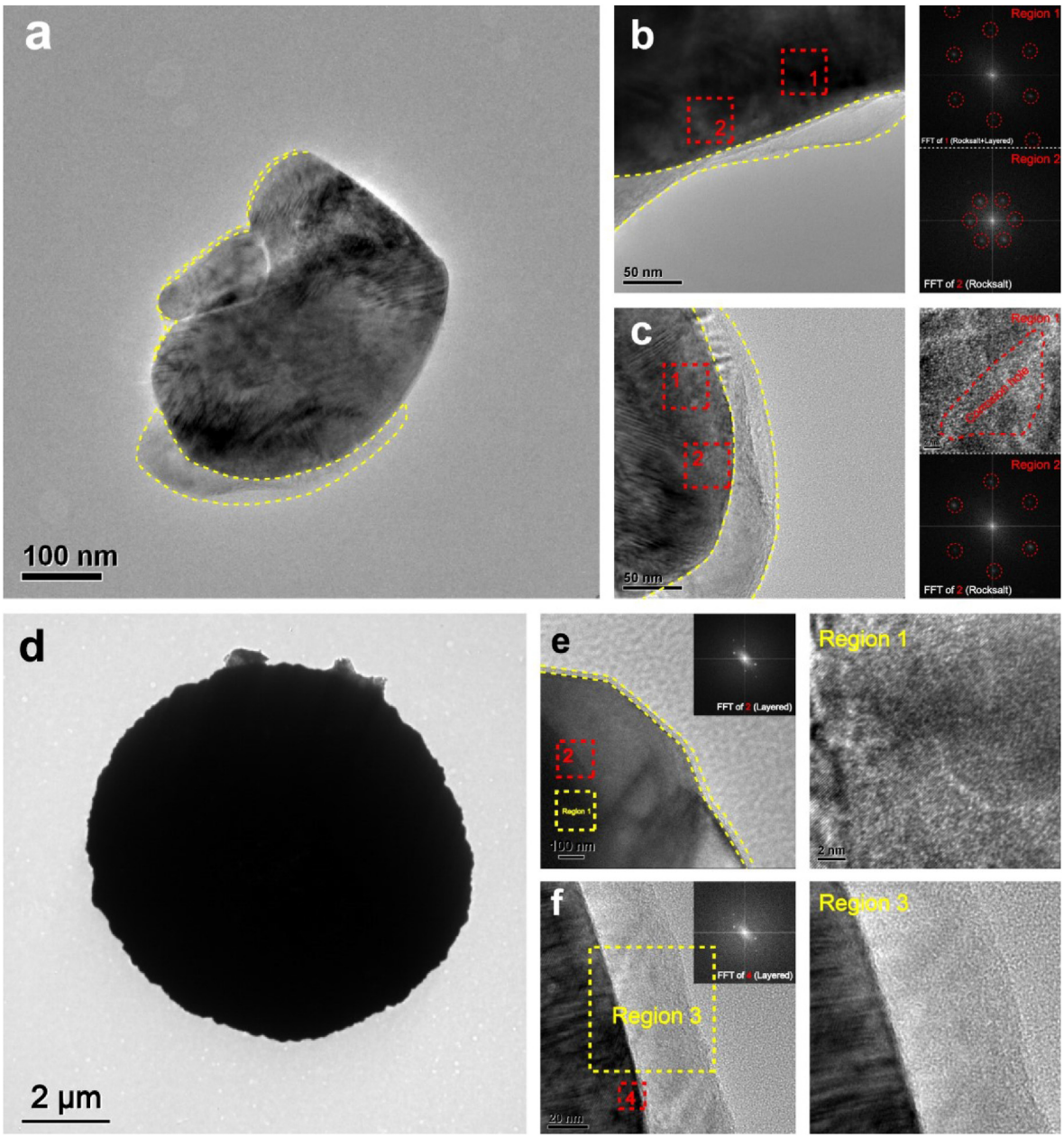

Fig. 6. TEM test results of NCM811 materials after 200 cycles in LB-301 (a–c) and SL (d–f) electrolytes.

pristine SiO_x-Gr anode material was composed of graphite flakes and SiO_x nanoparticles, and SiO_x nanoparticles were evenly dispersed and attached to the graphite sheets. After cycling in the LB-301 electrolyte (Fig. 7b), as observed in the SEM images (Fig. 5b), the SiO_x-Gr anode materials were significantly pulverized. At the same time, it is worth noting that compared to the fresh SiO_x-Gr anode materials, the size of SiO_x nanoparticles increased significantly after high-voltage long-cycle under LB-301 electrolyte conditions (Fig. 7b2), this may be due to the large volume expansion of SiO_x materials during the intercalation and deintercalation of lithium ion. In addition, some of the SiO_x nanoparticles were interconnected after cycling, which may be due to the mutual induction of SiO_x nanoparticles during the lithiation [45,46]. In contrast, this phenomenon does not occur when the SL electrolyte is used at high voltage. As can be seen from Fig. 7c1-7c2, under this condition, the morphology of the SiO_x-Gr anode materials was well maintained, the graphite sheet was still intact, and the size of SiO_x nanoparticles did not change significantly compared to the original material. The results further suggest that SL electrolyte can protect the structure of SiO_x-Gr materials under high voltage.

In order to further explore the changes of materials before and after cycling in different electrolytes, XRD tests were performed on NCM811 and SiO_x-Gr materials. From Fig. 8a, it is obvious that after a long cycle under high voltage, the NCM811 materials with the LB-301 electrolyte underwent irreversible phase transition [47–49], but the degree of phase change of the NCM811 materials was significantly lower when the SL electrolyte was used. This is also consistent with previous TEM test results. Furthermore, for ternary cathode materials, when the ratio of the peak intensities of (003) and (104) is larger in the XRD test, it means that the mixed cations in the materials are smaller and the layered structure of the material is more intact [50,51]. From Tab.S4, the peak intensity ratio of

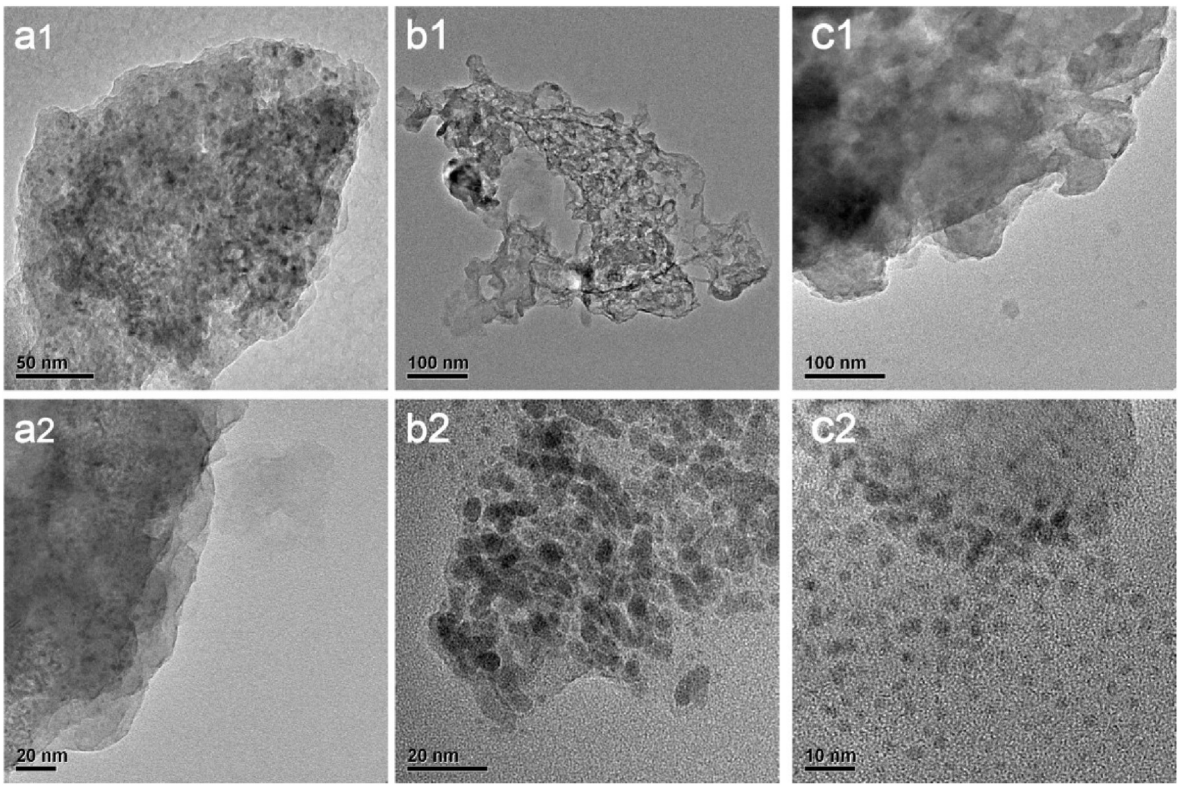

Fig. 7. TEM test results of the pristine SiO_x-Gr anode materials (a) and SiO_x-Gr anode after 200 cycles in the LB-301 (b) and SL (c) electrolytes, respectively.

(003) and (104) of the pristine NCM811 is the largest, followed by the cycled NCM811 in the SL electrolyte, and the peak intensity ratio of the cycled NCM811 with LB-301 electrolyte is the lowest. From the calculation results of XRD, the structure of the NCM811 materials after the circulation in the SL electrolyte is more intact.

What's more, what we cannot ignore is that the Raman test has a good detection effect on ternary cathode materials. If the intensity of the ratio of A_{1g} to E_g peak is higher, the structural integrity of the ternary material is stronger. In Fig. 8b and Tab.S4, although the A_{1g}/E_g value of the NCM811 materials after cycling in both electrolytes decreased, it is obvious that when using the SL electrolyte, the peak intensity ratio of A_{1g}/E_g in the Raman test is larger, and this conclusion is also in accordance with the previous XRD results.

Obvious corrosion holes appeared in Fig. 6c, which were caused by the dissolution of transition metal ions in cathode materials. In order to further verify this statement, EDS tests were performed on the cycled SiO_x-Gr electrodes to observe the content of transition metal ions on its surface. Fig. 8d is the result of SiO_x-Gr anode after working in the LB-301 electrolyte, the SiO_x-Gr anode circulated in the SL electrolyte is displayed in Fig. 8e. The test results confirm that the content of transition metal ions on the exterior of the anode materials after cycling in the LB-301 electrolyte is higher, indicating that the SL electrolyte is able to essentially prevent the dissolution of metal ions in NCM811 materials under high voltage.

In addition, XRD tests were also carried out on the SiO_x-Gr electrodes before and after cycling (Fig. 8c). Compared with the original SiO_x-Gr materials, the structure of the SiO_x-Gr materials after cycling in LB-301 changed more significantly, which is also in accordance with the previous TEM experiment results. In the XRD results of the SiO_x-Gr materials after cycled in the LB-301 electrolyte, the peak intensity around 43° was significantly enhanced, it may be because the SiO_x-Gr materials were severely crushed after recycling under this condition, which caused the copper current collector more exposed.

In order to clarify the states of the positive and negative electrode surfaces after high voltage cycling, XPS tests were performed on the cycled positive and negative electrodes. The F1s, P2p and S2p spectras of the positive electrode surface after 200 cycles under high voltage are shown in Fig. 8f–h. In the F1s spectrum, the peak of 685.0 eV belongs to LiF [52], and the peak near 687.5 eV corresponds to the substance of C–F [35]. In the P2p spectrum, the peaks at 136.6 eV and 133.5 eV are attributed to the decomposition products of $LiPF_6$ on the positive electrode surface, Li_xPF_y and $Li_xPF_yO_z$, respectively [53]. These are all the decomposition products of electrolyte. The results confirm that when the SL electrolyte was used, the peak strengths of the F and P elements on the surface of the positive electrodes were significantly weaker, which also indicates that the SL electrolyte was more stable at higher voltages and less prone to decomposition. For the S2p spectrum, it was only observed on the surface of positive electrodes in the SL electrolyte, indicating that just as we designed, sulfolane can effectively protect the NCM811 materials under high voltage. In fact, when the EDS test was performed on the positive electrode materials after one cycle at 4.5 V (Fig.S7), an obvious S element signal appeared on its surface. As mentioned before, in the EDS test of the negative electrode materials, it is found that when using LB-301, the content of transition metal ions on the negative electrode surface was significantly more. This result was also confirmed in the XPS test of the negative electrode surface. In the XPS test, the peak near 642 eV corresponds to the peak of Mn 2p3/2 [54]. The negative electrode in the LB-301 electrolyte showed a clear peak of Mn element on the surface, while it was almost not observed on the negative electrode surface in the SL electrolyte.

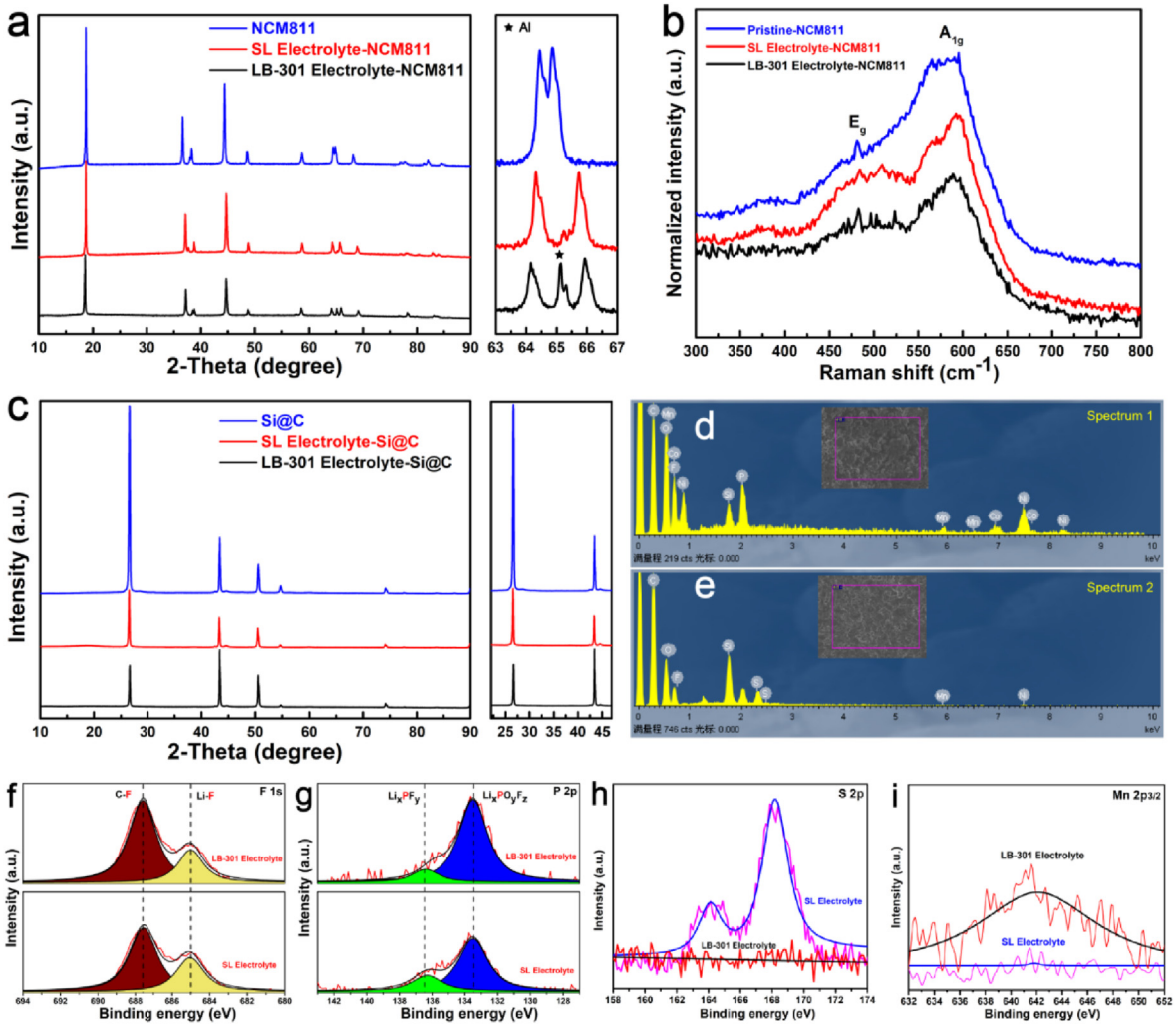

Fig. 8. XRD (a) and Raman (b) tests of NCM811 before and after 200 cycles in different electrolytes, XRD (c) and EDS (d) tests of SiO_x-Gr before and after 200 cycles in different electrolytes, XPS tests of NCM811 (f–h) and SiO_x-Gr (i) materials after 200 cycles in different electrolytes.

4. Conclusion

In summary, based on the theoretical calculations, a type of electrolyte is designed to effectively improve the high-voltage performance of the high-capacity NCM811/SiO_x-Gr system battery by taking advantage of each solvent components. In the designed electrolyte, the corresponding components can effectively protect the positive and negative materials during high voltage cycling, which greatly reduces the damage suffered by NCM811 and SiO_x-Gr materials under high voltage and significantly improves the cycling performance of the NCM811/SiO_x-Gr battery at high voltage. In addition, the conductivity of the electrolyte is very close to that of the conventional electrolyte, and its wettability is better with the separator than that of the conventional electrolyte. Therefore, this high-voltage electrolyte which takes advantage of various solvents may have a good application prospect in practical applications.

Declaration of competing interest

The authors declare that they have no known competing financial interests or personal relationships that could have appeared to influence the work reported in this paper.

CRediT authorship contribution statement

Xiangbang Kong: Methodology, Data curation, Writing - original draft. **Junjie Liu:** Data curation. **Yige Zhang:** Data curation. **Jing Zeng:** Writing - review & editing. **Jinbao Zhao:** Supervision.

Acknowledgements

We gratefully acknowledge the financial support of National Key Research and Development Program of China (2017YFB0102000), National Natural Science Foundation of China (21875198, 21875195), the Fundamental Research Funds for the Central Universities (20720190040), the National Found for Fostering Talents of Basic Science (J1310024).

Appendix A. Supplementary data

Supplementary data to this article can be found online at https://doi.org/10.1016/j.electacta.2020.136356.

References

[1] P.G. Bruce, Energy storage beyond the horizon: rechargeable lithium batteries, Solid State Ionics 179 (2008) 752–760, https://doi.org/10.1016/

j.ssi.2008.01.095.
[2] J.B. Goodenough, K.-S. Park, The Li-ion rechargeable battery: a perspective, J. Am. Chem. Soc. 135 (2013) 1167–1176, https://doi.org/10.1021/ja3091438.
[3] A. Manthiram, An outlook on lithium ion battery technology, ACS Cent. Sci. 3 (2017) 1063–1069, https://doi.org/10.1021/acscentsci.7b00288.
[4] J.W. Choi, D. Aurbach, Promise and reality of post-lithium-ion batteries with high energy densities, Nat. Rev. Mater. 1 (2016) 16013, https://doi.org/10.1038/natrevmats.2016.13.
[5] A. Ullah, A. Majid, N. Rani, A review on first principles based studies for improvement of cathode material of lithium ion batteries, J. Energy Chem. 27 (2018) 219–237, https://doi.org/10.1016/j.jechem.2017.09.007.
[6] X. Feng, et al., Time sequence map for interpreting the thermal runaway mechanism of lithium-ion batteries with LiNixCoyMnzO2 cathode, Frontiers in Energy Research 6 (2018), https://doi.org/10.3389/fenrg.2018.00126.
[7] Y.-S. Duh, K.H. Lin, C.-S. Kao, Experimental investigation and visualization on thermal runaway of hard prismatic lithium-ion batteries used in smart phones, J. Therm. Anal. Calorim. 132 (2018) 1677–1692, https://doi.org/10.1007/s10973-018-7077-2.
[8] A. Manthiram, J.C. Knight, S.-T. Myung, S.-M. Oh, Y.-K. Sun, Nickel-Rich and lithium-rich layered oxide cathodes: progress and perspectives, Advanced Energy Materials 6 (2016) 1501010, https://doi.org/10.1002/aenm.201501010.
[9] X. Kong, et al., Pre-blended conductive agent to effectively improve the storage properties of LiNi0.6Co0.2Mn0.2O2 cathode materials, J. Power Sources (2019) 227445, https://doi.org/10.1016/j.jpowsour.2019.227445.
[10] J.-Y. Li, et al., Research progress regarding Si-based anode materials towards practical application in high energy density Li-ion batteries, Mater. Chem. Front. 1 (2017) 1691–1708, https://doi.org/10.1039/C6QM00302H.
[11] D. Ma, Z. Cao, A. Hu, Si-based anode materials for Li-ion batteries: a mini review, Nano-Micro Lett. 6 (2014) 347–358, https://doi.org/10.1007/s40820-014-0008-2.
[12] L. Zhang, et al., Si-containing precursors for Si-based anode materials of Li-ion batteries: a review, Energy Storage Materials 4 (2016) 92–102, https://doi.org/10.1016/j.ensm.2016.01.011.
[13] L. Su, Z. Zhou, M. Ren, Core double-shell Si@SiO2@C nanocomposites as anode materials for Li-ion batteries, Chem. Commun. 46 (2010) 2590–2592, https://doi.org/10.1039/B925696B.
[14] H. Li, C. Liu, X. Kong, J. Cheng, Zhao, J. Prediction of the heavy charging current effect on nickel-rich/silicon-graphite power batteries based on adiabatic rate calorimetry measurement, J. Power Sources 438 (2019) 226971, https://doi.org/10.1016/j.jpowsour.2019.226971.
[15] H. Li, X. Kong, C. Liu, Zhao, J. Study on thermal stability of nickel-rich/silicon-graphite large capacity lithium ion battery, Appl. Therm. Eng. 161 (2019) 114144, https://doi.org/10.1016/j.applthermaleng.2019.114144.
[16] J. Wang, et al., Superconcentrated electrolytes for a high-voltage lithium-ion battery, Nat. Commun. 7 (2016) 12032, https://doi.org/10.1038/ncomms12032.
[17] Y. Tang, et al., Water-soluble sericin protein enabling stable solid-electrolyte interphase for fast charging high voltage battery electrode, Adv. Mater. 29 (2017), https://doi.org/10.1002/adma.201701828.
[18] Z. Chen, D. Chao, J. Lin, Z. Shen, Recent progress in surface coating of layered LiNixCoyMnzO2 for lithium-ion batteries, Mater. Res. Bull. 96 (2017) 491–502, https://doi.org/10.1016/j.materresbull.2017.05.021.
[19] Z. Liu, et al., Silicon oxides: a promising family of anode materials for lithium-ion batteries, Chem. Soc. Rev. 48 (2019) 285–309, https://doi.org/10.1039/C8CS00441B.
[20] H. Wu, Y. Cui, Designing nanostructured Si anodes for high energy lithium ion batteries, Nano Today 7 (2012) 414–429, https://doi.org/10.1016/j.nantod.2012.08.004.
[21] R. Hu, W. Sun, Y. Chen, M. Zeng, M. Zhu, Silicon/graphene based nanocomposite anode: large-scale production and stable high capacity for lithium ion batteries, J. Mater. Chem. A 2 (2014) 9118–9125, https://doi.org/10.1039/C4TA01013B.
[22] S.A. Delp, et al., Importance of reduction and oxidation stability of high voltage electrolytes and additives, Electrochim. Acta 209 (2016) 498–510, https://doi.org/10.1016/j.electacta.2016.05.100.
[23] X. Kong, R. Zhou, J. Wang, J. Zhao, An effective electrolyte strategy to improve the high-voltage performance of LiCoO2 cathode materials, ACS Appl. Energy Mater. 2 (2019) 4683–4691, https://doi.org/10.1021/acsaem.9b00149.
[24] C.-C. Su, et al., Oxidatively stable fluorinated sulfone electrolytes for high voltage high energy lithium-ion batteries, Energy Environ. Sci. 10 (2017) 900–904, https://doi.org/10.1039/c7ee00035a.
[25] W. Huang, et al., Dynamic structure and chemistry of the silicon solid-electrolyte interphase visualized by cryogenic electron microscopy, Matter 1 (2019) 1232–1245, https://doi.org/10.1016/j.matt.2019.09.020.
[26] P. Oh, B. Song, W. Li, A. Manthiram, Overcoming the chemical instability on exposure to air of Ni-rich layered oxide cathodes by coating with spinel LiMn1.9Al0.1O4, J. Mater. Chem. 4 (2016) 5839–5841, https://doi.org/10.1039/c6ta01061j.
[27] Z. Chen, et al., The high-temperature and high-humidity storage behaviors and electrochemical degradation mechanism of LiNi0.6Co0.2Mn0.2O2 cathode material for lithium ion batteries, J. Power Sources 363 (2017) 168–176, https://doi.org/10.1016/j.jpowsour.2017.07.087.
[28] A. Funabiki, M. Inaba, Z.A.c. Ogumi, Impedance analysis of electrochemical lithium intercalation into highly oriented pyrolytic graphite, J. Power Sources 68 (1997) 227–231, https://doi.org/10.1016/S0378-7753(96)02556-6.
[29] T. Liu, A. Garsuch, F. Chesneau, B.L. Lucht, Surface phenomena of high energy Li(Ni1/3Co1/3Mn1/3)O2/graphite cells at high temperature and high cutoff voltages, J. Power Sources 269 (2014) 920–926, https://doi.org/10.1016/j.jpowsour.2014.07.051.
[30] L. Imholt, et al., Trimethylsiloxy based metal complexes as electrolyte additives for high voltage application in lithium ion cells, Electrochim. Acta 235 (2017) 332–339, https://doi.org/10.1016/j.electacta.2017.03.092.
[31] M.D. Levi, et al., Solid-state electrochemical kinetics of Li-ion intercalation into Li[sub 1−x]CoO[sub 2]: simultaneous application of electroanalytical techniques SSCV, PITT, and EIS, J. Electrochem. Soc. 146 (1999), https://doi.org/10.1149/1.1391759.
[32] C.-G. Shi, et al., A special enabler for boosting cyclic life and rate capability of LiNi0.8Co0.1Mn0.1O2: green and simple additive, Nanomater. Energy 65 (2019) 104084, https://doi.org/10.1016/j.nanoen.2019.104084.
[33] H.H. Ryu, et al., Li[Ni0.9Co0.09W0.01]O2: a new type of layered oxide cathode with high cycling stability, Advanced Energy Materials (2019), https://doi.org/10.1002/aenm.201902698.
[34] L. de Biasi, et al., Chemical, structural, and electronic aspects of formation and degradation behavior on different length scales of Ni-rich NCM and Li-rich HE-NCM cathode materials in Li-ion batteries, Adv. Mater. (2019), e1900985, https://doi.org/10.1002/adma.201900985.
[35] H. Cai, H. Jing, X. Zhang, M. Shen, Q. Wang, Improving high-voltage performance of lithium-ion batteries with sulfolane as an electrolyte additive, J. Electrochem. Soc. 164 (2017) A714–A720, https://doi.org/10.1149/2.0801704jes.
[36] M.K. Jangid, et al., Effect of the presence of Si-oxide/sub-oxide surface layer(s) on 'micron-sized' Si wires towards the electrochemical behavior as anode material for Li-ion battery, Electrochim. Acta 297 (2019) 381–391, https://doi.org/10.1016/j.electacta.2018.11.201.
[37] X. Zhao, et al., Structure design and performance of LiNixCoyMn1-x-yO2 cathode materials for lithium-ion batteries, A Review 61 (2014) 1071–1083, https://doi.org/10.1002/jccs.201400107.
[38] S. Ma, et al., In situ formed LiNi0.8Co0.1Mn0.1O2@LiF composite cathode material with high rate capability and long cycling stability for lithium-ion batteries (2019), https://doi.org/10.1007/s11581-019-03353-2.
[39] U.H. Kim, et al., Pushing the limit of layered transition metal oxide cathodes for high-energy density rechargeable Li ion batteries, Energy Environ. Sci. 11 (2018) 1271–1279, https://doi.org/10.1039/c8ee00227d.
[40] H.H. Ryu, G.T. Park, C.S. Yoon, Y.K. Sun, Microstructural degradation of Ni-rich Li[nix coy Mn1 -x-y]O2 cathodes during accelerated calendar aging, Small 14 (2018), e1803179, https://doi.org/10.1002/smll.201803179.
[41] S.K. Jung, et al., Understanding the degradation mechanisms of LiNi0.5-Co0.2Mn0.3O2 cathode material in lithium ion batteries, Adv. Energy Mater. 4 (2014) doi:ARTN 130078710.1002/aenm.201300787.
[42] S. Liu, et al., Unraveling the capacity fading mechanisms of LiNi 0.6 Co 0.2 Mn 0.2 O 2 at elevated temperatures, J. Power Sources 393 (2018) 92–98, https://doi.org/10.1016/j.jpowsour.2018.05.029.
[43] S. Hwang, S.M. Kim, S.-M. Bak, K.Y. Chung, W. Chang, Investigating the reversibility of structural modifications of LixNiyMnzCo1−y−zO2 cathode materials during initial charge/discharge, at multiple length scales, Chem. Mater. 27 (2015) 6044–6052, https://doi.org/10.1021/acs.chemmater.5b02457.
[44] C.-H. Shen, et al., In situ multitechnical investigation into capacity fading of high-voltage LiNi0.5Co0.2Mn0.3O2, ACS Appl. Mater. Interfaces 8 (2016) 35323–35335, https://doi.org/10.1021/acsami.6b12597.
[45] M. Gu, et al., In situ TEM study of lithiation behavior of silicon nanoparticles attached to and embedded in a carbon matrix, ACS Nano 6 (2012) 8439–8447, https://doi.org/10.1021/nn303312m.
[46] K. Karki, et al., Lithium-assisted electrochemical welding in silicon nanowire battery electrodes, Nano Lett. 12 (2012) 1392–1397, https://doi.org/10.1021/nl204063u.
[47] M. Du, et al., Enhanced high-voltage cycling stability of Ni-rich LiNi0.8-Co0.1Mn0.1O2 cathode coated with Li2O−2B2O3, J. Alloys Compd. 805 (2019) 991–998, https://doi.org/10.1016/j.jallcom.2019.07.176.
[48] H. Li, et al., Stabilizing nickel-rich layered oxide cathodes by magnesium doping for rechargeable lithium-ion batteries, Chem. Sci. 10 (2019) 1374–1379, https://doi.org/10.1039/c8sc03385d.
[49] K.A. Pushnitsa, A.E. Kim, A.A. Popovich, Q. Wang, P.A. Novikov, Structural transformation of LiNi0.8Co0.1Mn0.1O2 cathode material during cycling with overcharge investigated by in situ X-ray diffraction, J. Electron. Mater. 48 (2019) 6694–6699, https://doi.org/10.1007/s11664-019-07489-9.
[50] X. Lu, et al., A modified co-precipitation process to coat LiNi1/3Co1/3Mn1/3O2 onto LiNi0.8Co0.1Mn0.1O2 for improving the electrochemical performance, Appl. Surf. Sci. 297 (2014) 182–187, https://doi.org/10.1016/j.apsusc.2014.01.121.
[51] T. Ohzuku, A. Ueda, M. Nagayama, Electrochemistry and structural chemistry of LiNiO2 (R3m) for 4 volt secondary lithium cells, J. Electrochem. Soc. 140 (1993), https://doi.org/10.1149/1.2220730.
[52] A.S. Wotango, et al., Improved interfacial properties of MCMB electrode by 1-(trimethylsilyl)imidazole as new electrolyte additive to suppress LiPF6 decomposition, ACS Appl. Mater. Interfaces 9 (2017) 2410–2420, https://doi.org/10.1021/acsami.6b13105.
[53] H. Rong, et al., A novel imidazole-based electrolyte additive for improved electrochemical performance of high voltage nickel-rich cathode coupled with graphite anode lithium ion battery, J. Power Sources 332 (2016) 312–321, https://doi.org/10.1016/j.jpowsour.2016.09.016.
[54] M.A. Stranick, Mn2O3 by XPS, Surf. Sci. Spectra 6 (1999) 39–46, https://doi.org/10.1116/1.1247889.